Asian Journal of Advanced Research and Reports

6(2): 1-20, 2019; Article no.AJARR.51494

Modelling Secular Variation in the Southwest Pacific

Maha Ali Alfheid[1*] and Mohana Faroug Attia[1]

[1]Alasala Colleges/Colleges of Engineering, P.O.Box 2666, Dammam, 31483, Saudi Arabia.

Authors' contributions

This work was carried out in collaboration between both authors. Author MAA designed the study, performed the statistical analysis, wrote the protocol and wrote the first draft of the manuscript. Author MFA managed the analyses of the study. Author MFA managed the literature searches. Both authors read and approved the final manuscript.

Article Information

DOI: 10.9734/AJARR/2019/v6i230150
Editor(s):
(1) Dr. Azizur Rahman, Department of Chemical & Physical Sciences, University of Toronto, Davis Building, Canada.
Reviewers:
(1) Sie Long Kek, Universiti Tun Hussein Onn Malaysia, Malaysia.
(2) Pasupuleti Venkata Siva Kumar, Vallurupalli Nageswara Rao Vignana Jyothi Institute of Engineering & Technology, India.
(3) Lourenildo W. B. Leite, Federal University of Pará, Brazil.
Complete Peer review History: http://www.sdiarticle4.com/review-history/51494

Original Research Article

Received 25 July 2019
Accepted 27 September 2019
Published 03 October 2019

ABSTRACT

A spherical cap harmonic analysis (SCHA) model has been used to derive a high resolution regional model of the geomagnetic field in the southwest Pacific region over the past 400 years. Two different methods, a self-consistent and the *gufm1* dipole method, have been used to fill in gaps in the available data. The data used in the analysis were largely measurements of the magnetic field recorded in ships logs on voyages of exploration in the region. The method chosen for the investigation used a spherical cap of radius θ_0= 50° centered at co-latitude and longitude of (115°,160°). The results of each method used for SCHA are presented as contour plots of magnetic field declination, inclination and intensity and are compared with similar plots for a global model, *gufm1*. The root mean square misfit of the self- consistent and *gufm1* dipole model to the actual data were around 2900 nT and 23000 nT respectively. Overall, the results suggest that the self-consistent model produces a more reliable model of the geomagnetic field within the area of interest than does the *gufm1* dipole model. With more data included the self-consistent model could be further improved and used to develop a high resolution mathematical model of the geomagnetic field in the southwest Pacific region.

Keywords: Southwest pacific; geomagnetic field; gufm1; spherical harmonic analysis.

**Corresponding author: Email: maha.alfheid@alasala.edu.sa;*

1. INTRODUCTION

William Gilbert was the first person who identified, in his book De Magnete, that the Earth's magnetic field is a property of the Earth itself. It originates from an active, self-sustaining dynamo operating in the liquid outer core of metallic composition [1]. The Earth's magnetic field can be approximated by a magnetic dipole tilted at an angle of about 11 degrees from the Earth's rotational axis. Such a dipole accounts for roughly 90% of the present day geomagnetic field at any point on the Earth's surface. The measured field shows that the dipole is oriented towards the south rotation pole, so that the field has an upward component in the southern hemisphere and a downward component in the northern hemisphere. The remaining approximately 10% of the field is termed the non-dipole field. Both the dipole and the non-dipole fields contribute to the overall pattern of the Earth's magnetic field and they both vary with time [2]. The Earth's magnetic field at any location on the surface of the Earth is a vector which can be represented in terms of "three parameters: Declination "D", Inclination "I" and Intensity "F"." as shown in Fig. 1, which comes from [2].

The declination is the angle between the horizontal component of the magnetic field and true north, the inclination is the angle the field makes with the horizontal and *F* is the intensity or magnitude of the field. Inclination is 90º at the north magnetic Pole and -90º at the south magnetic pole. Due to the changing non-dipole field, the north and south magnetic poles move around independently of each other and they are not directly opposite each other. Maxwell's equations of electromagnetism can be used to obtain a mathematical model to describe the geomagnetic field. Two reasonable assumptions are that the atmosphere is an insulator and that it is non-magnetic. As a result, the geomagnetic field is normally measured in a region, between the surface of the Earth and the ionosphere, in which there are no electric currents and no magnetic sources. In this region, where there are no currents or sources of the magnetic field, the field can be expressed as the gradient of a scalar magnetic potential (U), such that;

$$B = -\nabla \mathrm{U} \tag{1}$$

The Maxwell equation, stating that;

$$\text{div B} = 0 \tag{2}$$

therefore, implies that the scalar magnetic potential obeys Laplace's equation at the surface of the Earth.

$$\nabla^2 U = 0 \tag{3}$$

Solving Laplace's equation in spherical polar coordinates (*r, θ, φ*) gives a method of modeling the magnetic scalar potential of the Earth's magnetic field. Although this is only strictly applicable in the region between the surface and the ionosphere, it is often also applied within the Earth, for example to look at the field on the core-mantle boundary. This involves the assumption that the mantle can be treated as an insulator. Solving Laplace's equation can also, provide a way of modeling the vector field on a restricted area on the surface of the earth. The main field of the Earth is entirely of internal origin and the solution of Laplace's equation in spherical polar coordinates, known as a Spherical Harmonic Analysis (SHA) is in the form;

$$U(r,\theta,\emptyset) = a\sum_{l=1}^{\infty}\sum_{m=0}^{l}\left(\frac{a}{r}\right)^{l+1} (g_l^m cos\, m\phi + h_l^m \sin m\phi) p_l^m (cos\theta) \tag{4}$$

where *r* is the distance of the observational point from the center of the Earth and θ, $\emptyset$ are the colatitude and longitude of the observational point, respectively, *a* is the radius of the Earth, and g_l^m and h_l^m have the same dimensions as B (i.e. SI units are Tesla) and are referred to as Gauss coefficients. The p_l^m *(cos*θ) are Schmidt-normalized associated Legendre polynomials, and divide the meridian, or longitudinal line, into *l-m+1* zones of alternate signs. The *cos* $m\phi$ or *sin* $m\phi$ terms divide the longitudinal line into 2m longitudinal sectors of alternate signs at equal intervals *π/m*. The product of the Legendre polynomials with the *cos* $m\phi$ or *sin* terms divide up the surface of the sphere into regions created by the latitude zones and longitude sectors. It also gives surface spherical harmonics which vary with θ and ϕ with degree *l* and order m and show the symmetry of the various contributions to the geomagnetic field at the surface of the Earth [3]. Each harmonic is equivalent to a particular arrangement of magnetic poles at the center of the Earth. The lowest degree of Gauss coefficient is g_0^0 which would correspond to *l=0* and *m=0*, i.e. a monopole.

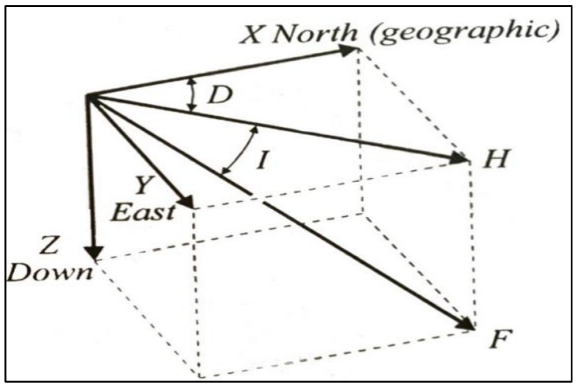

Fig. 1. The geomagnetic field elements, The Inclination, I, shows the inclined angle of the field below the horizontal, the declination, D, is the angle between geomagnetic north and true north and the intensity magnitude of the field, F

As *div B = 0* implies that isolated magnetic monopoles do not exist, this term does not appear in Equation 4 in which the summation starts at *l=1*. The next three coefficients g_1^0, g_1^1 and h_1^1 define the direction and magnitude of the geocentric dipole, which is equivalent to two opposing charges brought close together [3]. These terms give the first approximation to the observed geomagnetic field. The spherical harmonic terms with *l=2* describes the best fitting geocentric quadrupole, which is equivalent to two dipoles brought together, and the terms with l =3 describe the best fitting geocentric octupole and so on for higher degree terms [2]. Gradual changes of the Earth's magnetic field on a time scale of a year or more are referred to as geomagnetic secular variation. The variations of the magnetic field on a time scale shorter than about a year are caused by sources of external origin, largely due to the changing intensity of the solar wind. The longer time scale variations are of internal origin due to the continual motion of the Earth's fluid outer core [4]. Secular variation can be described by continuous changes of small amplitude with periodicities ranging from a year to 100,000 years. However, the polarity of the main dipole reverses on time scales from hundreds of thousands to a million years, changing the north pole to the south pole and the south pole to the north pole [2,3]. Henry Gellibrand was the first to note the fact that the geomagnetic field is not constant. He found that the declination in London had decreased from 11.3°E to 4.1°E between 1580 and 1634. The historical dataset describes secular variation in terms of three phenomena. First, a steady decay in the magnetic moment of the dipole, which is described by the derivative $\frac{\partial g_1^0}{\partial t}, \frac{\partial g_1^1}{\partial t}$ and $\frac{\partial h_1^1}{\partial t}$. Second, an overall westward drift of the non-dipole field with a drift rate estimated by Bullard (1950) of about 0.18° / yr. Third, a slow westward movement of the geomagnetic poles, which is described by $\frac{\partial g_2^0}{\partial t}$. The magnitude of the secular variation is also observed to be generally smaller over the Pacific hemisphere and the non-dipole field weaker [3]. The standard mathematical model of the geomagnetic field, called the International Geomagnetic Reference Field (IGRF), is revised every five years and is based on Spherical Harmonic Analysis (SHA), which is described in more detail in geomagnetic field analysis is and description. This study concerns the southwest Pacific region and deals with developing a mathematical model of the geomagnetic field specific to this area. Models of the Earth's magnetic field from SHA using only observations in the southwest Pacific are of low accuracy, while models determined using SHA with a full global data are of low resolution in the southwest Pacific [5]. Therefore, a Spherical Cap Harmonic Analysis (SCHA), which is a technique specifically designed to produce a model only for a local region will be used. Over small or large areas from a few to many millions of square kilometer, SCHA is preferable to SHA for modeling the magnetic field in a restricted region [6].

2. MATERIALS AND METHODS

2.1 Study Design and Site

The spherical cap in this study chosen covers the southwest Pacific region has a radius of 50° and is centered on latitude 25°S, longitude

160°E. This cap covers New Zealand, Australia and a significant portion of the Antarctica region.

2.2 Data Collection

The data used in determining the regional model of the magnetic field, which is applicable only for the southwest Pacific region, was also used in the *gufm1* model which is based on a large amount of historical magnetic field observational data from 1590 to 1990 [7].

2.3 Geomagnetic Field Analysis and Description

2.3.1 Spherical harmonic analysis

Spherical Harmonic Analysis (SHA) is a method used to study any quantity that varies upon the surface of the sphere [8]. Spherical Harmonic Analysis has been applied to various types of data. The SHA technique is normally used to determine the magnetic potential when data are available over the whole earth.

2.3.2 Spherical cap harmonic analysis

SCHA gives a regional model designed to represent the magnetic field in a particular portion of the earth's surface – either when a high proportion of the observations are in a particular region, or because of special interest to study the field over a certain area [9]. SCHA is also used in modeling other applications like regional secular variation [10] the crustal magnetic anomaly field and in modeling sea level data [11].

2.3.3 Method of solution

To calculate the Gauss coefficients of the SCHA models, the magnetic field components must be fit over the spherical cap. Expressions for B_x, B_y and B_z at each site location are dependent on θ_T and $\emptyset_T$, the latitude and longitude respectively, of the site, the Gauss coefficients, and the ratio of a to *r*. As all data had been measured on the surface of the Earth then *a*=*r*, and so the radial dependence cancels out. A MATLAB computer program has been used to calculate a least squares best fit to the input data.

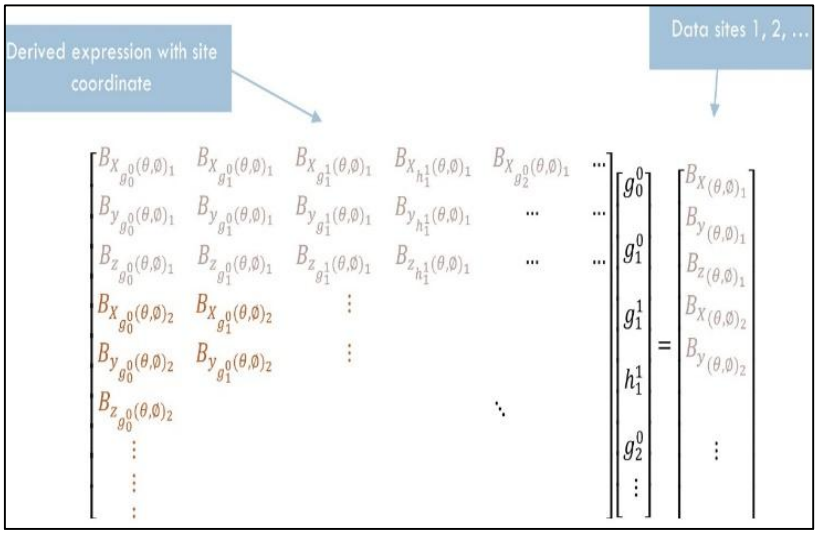

(5)

2.3.3.1 Cap reference frame

where the $B_X g_l^m{}_{(\theta,\emptyset)s}$, $B_y g_l^m{}_{(\theta,\emptyset)s}$, $B_z g_l^m{}_{(\theta,\emptyset)s}$, $B_X h_l^m{}_{(\theta,\emptyset)s}$,$B_y h_l^m{}_{(\theta,\emptyset)s}$ and $B_z h_l^m{}_{(\theta,\emptyset)s}$ are the spatial terms of the *l* degree and *m* order. The *g's* and *h's* are the calculated Gauss coefficients at the measurement site $(\theta, \emptyset)$ *s*. The "B_x $(\theta, \emptyset)$, B_y $(\theta, \emptyset)$, B_z $(\theta, \emptyset)$" are the magnetic field measurements.

2.3.3.2 Geographic reference frame

To calculate the Gauss coefficients from this matrix inversion, all historical data recorded in terms of declination, inclination and intensity should be converted to B_x, B_y and B_y first. From Fig. 1 we can find that:

$$B_x = F \cos I \cos D$$
$$B_y = F \cos I \sin D \quad (6)$$
$$B_z = F \sin I$$

The matrix inversion was carried out using MATLAB a program sc2ver2.m written by Ingham [12] which takes as input the latitude, longitude of each site and B_x, B_y and B_z at the site in geographic coordinates, does the coordinate and field transformations, calculates the SCHA and then converts back into geographic coordinates.

2.3.3.3 The geomagnetic field model "gufm1"

A brief description of the *gufm1* model [13] is included as part of the analysis in this paper involves comparisons with this model. The *gufm1* model provides the most complete picture of the geomagnetic field evaluation from 16th century onwards. Jackson et al. [13] constructed a continuous time-space magnetic field model with a global SHA model based on a large number, about 91000, of historical observations. From the magnetic potential equation;

$$U(r,\theta,\emptyset) = a\sum_{l=1}^{1}\sum_{m=0}^{1}\left(\frac{a}{r}\right)^{l+1}\left(g_l^m(t)\cos m\phi + h_l^m(t)\sin m\phi\right)p_l^m(\cos\theta) \quad (7)$$

where $g_l^m(t)$ and $h_l^m(t)$ are the Gauss coefficients as a function of time expanded to fourth order using B-spline basis functions $B_n(t)$ such that

$$g_l^m(t) = \sum_n g_l^{nm} B_n(t) \quad (8)$$

$$h_l^m(t) = \sum_n h_l^{nm} B_n(t) \quad (9)$$

where the $B_n\ t > 0$ if the $t \in |t_n, t_{n+4}|$ and zero otherwise. The magnetic field components therefore will be:

$$B_r = \sum_{l=1}^{\infty}\sum_{m=0}^{1}(l+1)\left(\frac{a}{r}\right)^{l+2}\left(g_l^m(t)\cos m\phi + h_l^m(t)\sin m\phi\right)p_l^m(\cos\theta) \quad (10)$$

$$B_\theta = -\sum_{l=1}^{\infty}\sum_{m=0}^{1}\left(\frac{a}{r}\right)^{l+2}\left(g_l^m(t)\cos m\phi + h_l^m(t)\sin m\phi\right)p_l^m\ \frac{dp_l^m(\cos\theta)}{d\theta} \quad (11)$$

$$B_\phi = \frac{1}{\sin\theta}\sum_{l=1}^{\infty}\sum_{m=0}^{1} m\left(\frac{a}{r}\right)^{l+2}\left(g_l^m(t)\cos m\phi + h_l^m(t)\sin m\phi\right)p_l^m(\cos\theta) \quad (12)$$

Jackson et al. [13] constructed this model to fit the input data smoothly in both time and space. Given the large number of declination observation before 1800, Jackson et al. used the decay of the dipole coefficients $g_0^1(t)$ with time to estimate intensity values before 1800. Spherical harmonic expansions, equation;

$$\phi_T = \sin^{-1}\left[\frac{\sin\theta_p \sin(\phi_c - \phi_p)}{\sin\theta_T}\right] \quad (13)$$

As $\sin^{-1}$ produces angles from -90 to 90, Quadrant $\emptyset_T$ should be in according to the relative values of $\emptyset_p$, $\emptyset_c$, $\emptyset_p$, $and\ \emptyset_c$.

Were truncated at *l = 14* to obtain the smoothest model and give the best representation of the field. Two model norms are used in the *gufm1* model, one measuring the roughness in the spatial domain, based on Gubbins [14] and the other roughness in the time domain.

2.4 Input Data

The data used to calculate a mathematical model of the field are normally made up of measurements of declination, inclination and intensity at different latitude and longitude. The data used in this study are those recorded by the explorers and traders who sailed in the southwest Pacific. These cover a period of time extending from Abel Tasman's discovery of Van Diemen's Land and New Zealand in the 17th century up to the Antarctic Explorations in the 19th century [15]. Even though inclination was recognized around 1600 by "Robert Norman (Norman, 1720)", few inclination data were recorded in the ships' logs and most of these data were in the late 18th century and few before that as shown in Fig. 2. The reason for this was partly the difficulty of measuring inclination whilst on a ship, also, inclination was not used in navigation as declination was at that time [12]. Von Humboldt made relative intensity measurements in South America in 1798 and intensity data start to appear in the southwest Pacific about the same time as shown in Fig. 2. The method of measurement was by timing the oscillations of the ship's dip needle [16]. Elisabeth Paul Edourd De Rossel made the first magnetic intensity measurements recorded in the southwest Pacific during 1791-1794 [17]. He measured the magnetic field intensity as a relative intensity referenced to a set location. For instance, all intensities data measured on the D'Entrecasteaux expeditions in 1792 while sailing throughout the Pacific were referenced to the intensity measured in Paris [18]. In this study, all intensities have been converted to absolute intensity in nano-tesla.

2.4.1 Difficulties of study

There were several problems that cause errors and uncertainties in taking measurements of magnetic data. These problems include the disturbance of the ship's iron on the magnetic instruments. This was accounted for by taking measurements in different places upon the ship with different magnetic instruments while in a port with a land-based measurement for comparison. Most of the voyages at this time also carried supplementary dip needles for inclination and intensity measurements in order to avoid error arising from any damage to an instrument during the voyage. The difficulty of determining the absolute position of a ship in the open ocean had been one of the major problems since the 16th century.

Fig. 2 shows the temporal distribution of the observed data (declination, inclination and intensity) used for the time interval 1600 to 1910.

Most of the data in the earliest epoch were declination-only data and were collected by Abel Tasman on his journey to discover the Van Diemen's Land and New Zealand in 1642 [19]. The distribution of the data in southwest Pacific is inhomogeneous, so to visualize the number of the data centered on various times in the interval 1600 to 1910, the spatial distribution of the data in each period of time has been mapped as shown in Fig. 3. The data have been divided up into different time intervals centered on the dates shown in the figure. Thus (a) in the figure is centered on 1633 and contains 113 observational data from 1606 to 1643. All these data are declination only and most of them are concentrated south and east of Australia, north of New Zealand, and some north of Papua New Guinea. Fig. 3(b) is centered on 1700 and contains 88 data from 1685 to 1710. Again all are declination. These data are confined southwest of Australia and few in the Pacific Ocean. Fig. 3(c) is centered on 1773 and contains 226 declination and 3 inclination data from 1765 to 1780. These data are mostly in the region north and east of Australia and around New Zealand. Fig. 3b(d) is for 1790 and it contains 491 declinations, 3 inclinations and one intensity data from 1786 to 1793 from all around the Pacific Ocean in the study area. Fig. 3 (e) is centered on 1825 and contains 254 declinations, 286 inclinations and 177 intensity data from 1805 to 1849. These data are concentrated mostly south of Australia and north of New Zealand. Fig. 3(f) is for 1875 and it contains 365 declinations, 148 inclinations and 138 intensity data from 1850 to 1890. These data are concentrated between Australia and New Zealand and around the Papua New Guinea. Fig. 3(g) is for 1900 and contains 44 declinations and 29 inclinations data from 1900 to 1949, but mainly from 1900 to 1910. The majority of these data come from the magnetic survey of New Zealand.

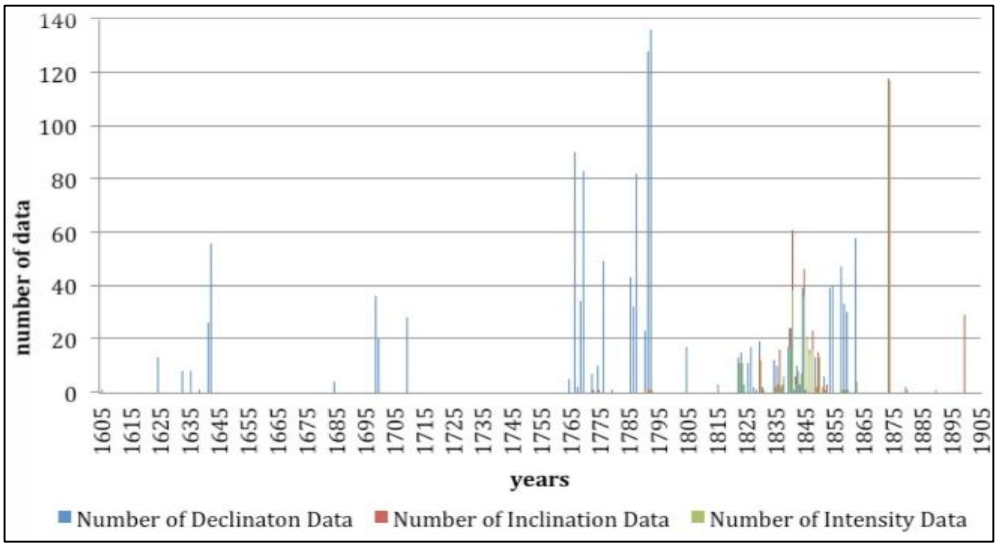

Fig. 2. Histogram of the number of measurements and temporal distributions of data taken from ships' logs. Blue represents declination data, red inclination data and green intensity data from 1600 to 1910

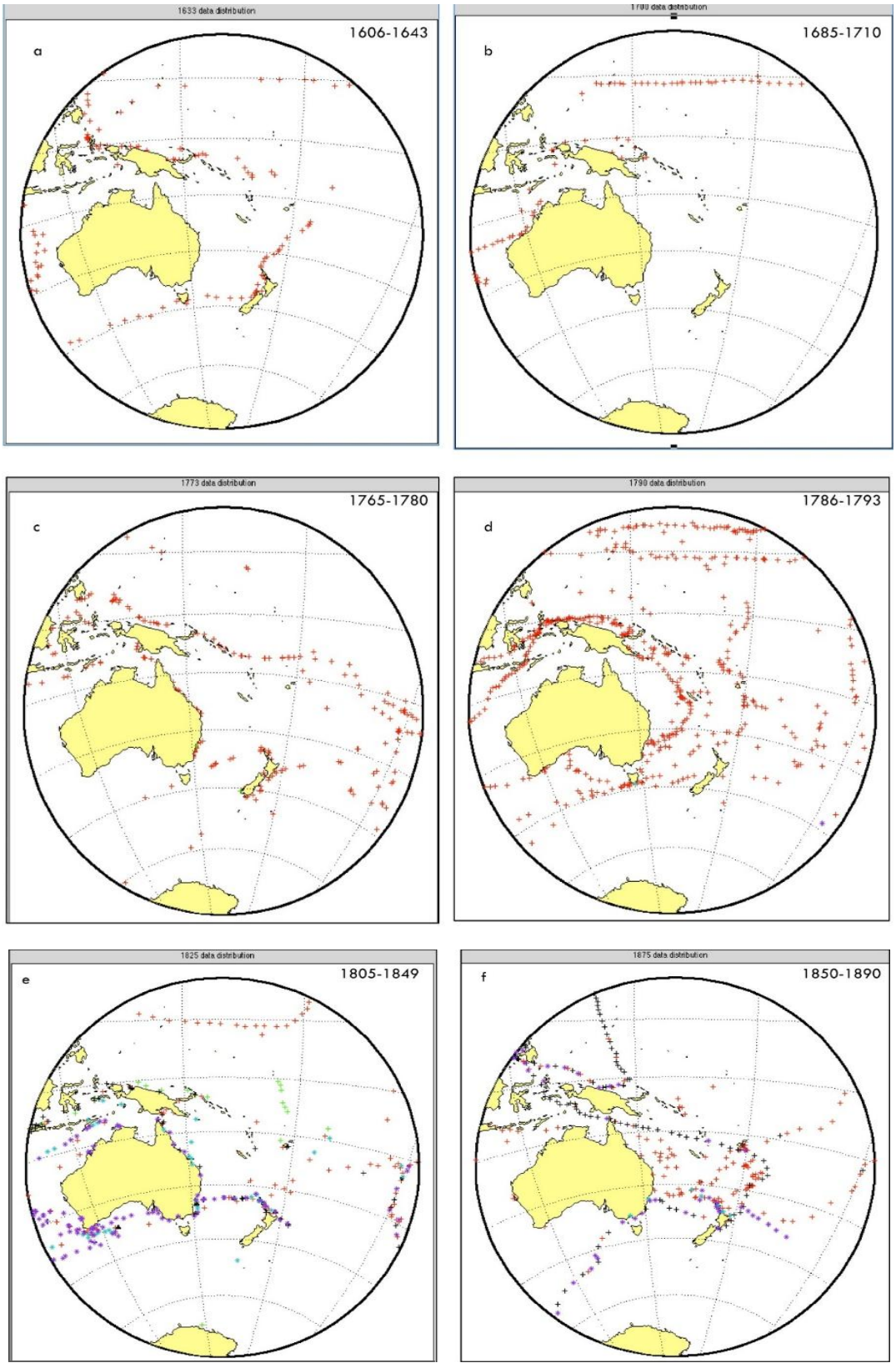
1633 data distribution
a
1606-1643
b
1685-1710
1773 data distribution
c
1765-1780
1790 data distribution
d
1786-1793
1825 data distribution
e
1805-1849
1875 data distribution
f
1850-1890

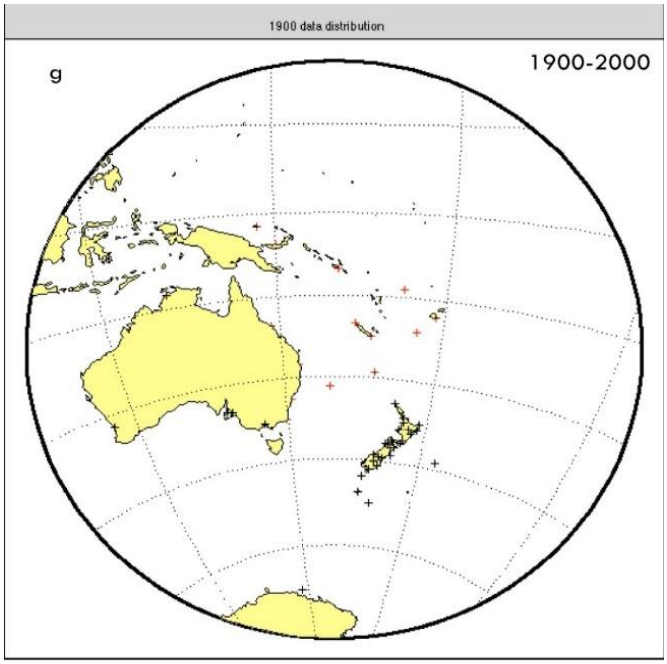

Fig. 3. Spatial distributions of the input data in the interval 1600 to 1910. + are data with declinations only, + are data with declinations and inclinations, * are data with inclinations only, * are data with inclinations and intensities, and + are data with declinations, inclinations and intensities. Projection is stereographic

2.4.2 Methods of analysis

The observational data are greatly biased towards declination measurements (Fig. 2) since before Gauss deduced his method of determining intensity in 1832 [7]. There are few intensity data in ships' records. Although there are a few inclination and intensity measurements, they are not as common. A full SCHA needs Bx, By and Bz data therefore where there are gaps in the record, a sensible method of mathematical estimation is required to fill the gaps. As the data distribution is not very even, this division has been chosen in a way that gives some consistency between amount of data in each epoch of SCH models. Taking into account the number of input data for each epoch, the epochs are labeled as follows:

1. 1633, which includes 113 observation data from 1606 to 1643. Fig. 3(a).
2. 1700, which includes 88 observation data from 1685 to 1710. Fig. 3(b).
3. 1773, which includes 284 observation data from 1765 to 1780. Fig. 3(c).
4. 1790, which includes 446 observation data from 1786 to 1793. Fig. 3(d).
5. 1825, which includes 717 observation data from 1805 to 1849. Fig. 3(e).
6. 1875, which includes 655 observation data from 1850 to 1890 Fig. 3(f).
7. 1900, which includes 44 observation data from 1900 to 1949. Fig. 3(g) with additional simulated measurement points added from the 1900 IGRF.

Simulated measurements from the IGRF have also been used for 1950 and 2000 to calculate SCHA models. This dataset has been compiled using two methods. One method uses the dipole coefficients of the *gufm1* model to estimate the unrecorded magnetic field components and it will be referred to as *gufm1* dipole coefficients method. The other method depends only on the observational data and will be referred to as the self-consistent analysis method. Each of these techniques is used to produce a SCHA model of each epoch and the results of this method of SCHA are compared with what the SHA based *gufm1* model itself gives for the field.

3. RESULTS AND DISCUSSION

3.1 Results of GUFM1 Dipole Model

As the *gufm1* model is the accepted global model representing the magnetic field since 17th

century, it makes sense to compare results of the gufm1 dipole model with it. In this study, nearly 1484 data points with data gaps filled using *gufm1* dipole data have been used with 343 actual observational data, giving a total of 1827 data in all. Results of the SCH models are shown as a series of contour plots of declination, inclination and intensity for each period of time.

3.1.1 Declination plots

The declination plots for the gufm1 dipole and gufm1 model have been presented side by side to test the reliability of gufm1 dipole technique for the time from 1633 to 2000. The major points of comparison can be broken down into four main points, From "Fig. 4":

1. There is quite a good agreement between the *gufm1* dipole and *gufm1* models for the time 2000 to 1950, Fig. 4 [A, J and B, K]. This was expected because both models are based largely on the same, quite well distributed data- complete (IGRF).
2. This agreement gets worse further back in time. An example of this is indeed the declination for 1700, Fig. 4 [H, R], and the reason for this is not only the small amount of data but also the complete lack of data around New Zealand for this epoch. For all the epochs prior to 1825 the declination plots tend to be similar where there is a reasonable distribution of data (e.g. in 1790 [F, O]) and dissimilar for 1773,1633 [S, P-I, Q] respectively, where there is a poor distribution of data.
3. The *gufm1* gives much larger negative declinations south of Australia than does the *gufm1* dipole model.
4. The change in declination across Australia is very similar in both and the values vary between -5 to +15. These values are in agreement with values of radiocarbon age recorded in lake sediments at Keilambete lake, south east Australia [20].

The *gufm1* is based on calculating time dependence of Gauss coefficients which results in quite smoothly changing models from epoch to epoch. The way of modeling used in the gufm1 dipole model does not guarantee the same smoothness, which is why results for 1700, 1773 and 1633 are so affected by a poor data distribution.

3.1.2 Inclination plots

As for the declination plots, inclination has been presented for both models in the same epochs. Inclination values in Fig.5 are negative in New Zealand and Australia. Inclination values given by the *gufm1* dipole model are compatible with those of *gufm1*. Inclinations in New Zealand vary from -72° to -63°. The *gufm1* dipole model gives more rapid change of inclination north of Australia with values 20° different from the *gufm1* model. The *gufm1* dipole model gives inclination contours, which tend to be flatter than in *gufm1*, especially around New Zealand. The exception is for 1700 where most of the data are in the far north of the spherical cap, Fig. 5.

Four main points can be made from the comparison between the self-consistent and gufm1 models for the time between 1900 to 1633 in the southwest Pacific region, Fig. 6.

3.1.3 Inclination Plots

The inclination plots for both the self-consistent and *gufm1* models are shown in Fig. 7 for the time from 1633 to 1900. No major differences are observed between the self-consistent and global *gufm1* models for inclination in the time period considered. The inclination plots from the self-consistent model show generally slightly lower values over New Zealand and adjacent areas than the *gufm1* models, especially between 1633 and 1790. All the self-consistent plots show a maximum inclination value reaching close to +50° in the north Pacific region where the maximum values in the *gufm1* model reach only to $+30^0$ ~ $+35^0$. In New Zealand, the inclination given by both models increases slowly going backwards in time. This increase agrees with the inclination variation found by G. M. Turner & Lillis [21] from palaeomagnetic lake sediment data.

3.2 Comparison of the Two Models

To investigate and assess the usefulness of the, self-consistent and *gufm1* dipole models, a comparison between these models has been made. The declination plots for the gufm1 dipole model show poor field prediction in the study area in period between 1650-1800. The declinations from both models are reasonably similar from 1825 onwards although the declinations for the self-consistent model are about ~5^0 higher than for the *gufm1* dipole model. The self-consistent model declinations

are also more like *gufm1* over most of the area. The inclination plots for both the *gufm1* dipole and self-consistent models are similar although the inclination values for the gufm1 dipole model are about ~5^0 steeper than for the self-consistent model before about 1775. Intensity contours for the *gufm1* dipole model do not appear realistic from 1633 until around 1775. Contours after this epoch are of similar shape to those from the self-consistent model. Overall, the intensity values at equatorial and high latitudes for the self-consistent model are higher by about ~25000 nT than for the *gufm1* dipole model. It appears that the declination, inclination and intensity values from the self-consistent model have a closer similarity to *gufm1* global SHA although there are some differences. Although contour plots of declination, inclination and intensity of both the *gufm1* dipole and self-consistent models are interesting and visual, they do not clearly show which is the better model to describe the field in our area of interest. Therefore, in order to investigate the reliability of both models, the misfit to the data has been calculated for each period of time from 1633 to 1875, Table 1. The values are the root mean squared difference between the magnetic field values (B_{Xe}, B_{Ye}, B_{Ze}) which have been used to calculate the SCHA model, and the predicted magnetic field value calculated from the final SCHA model coefficients at the latitude and longitude of each data point.

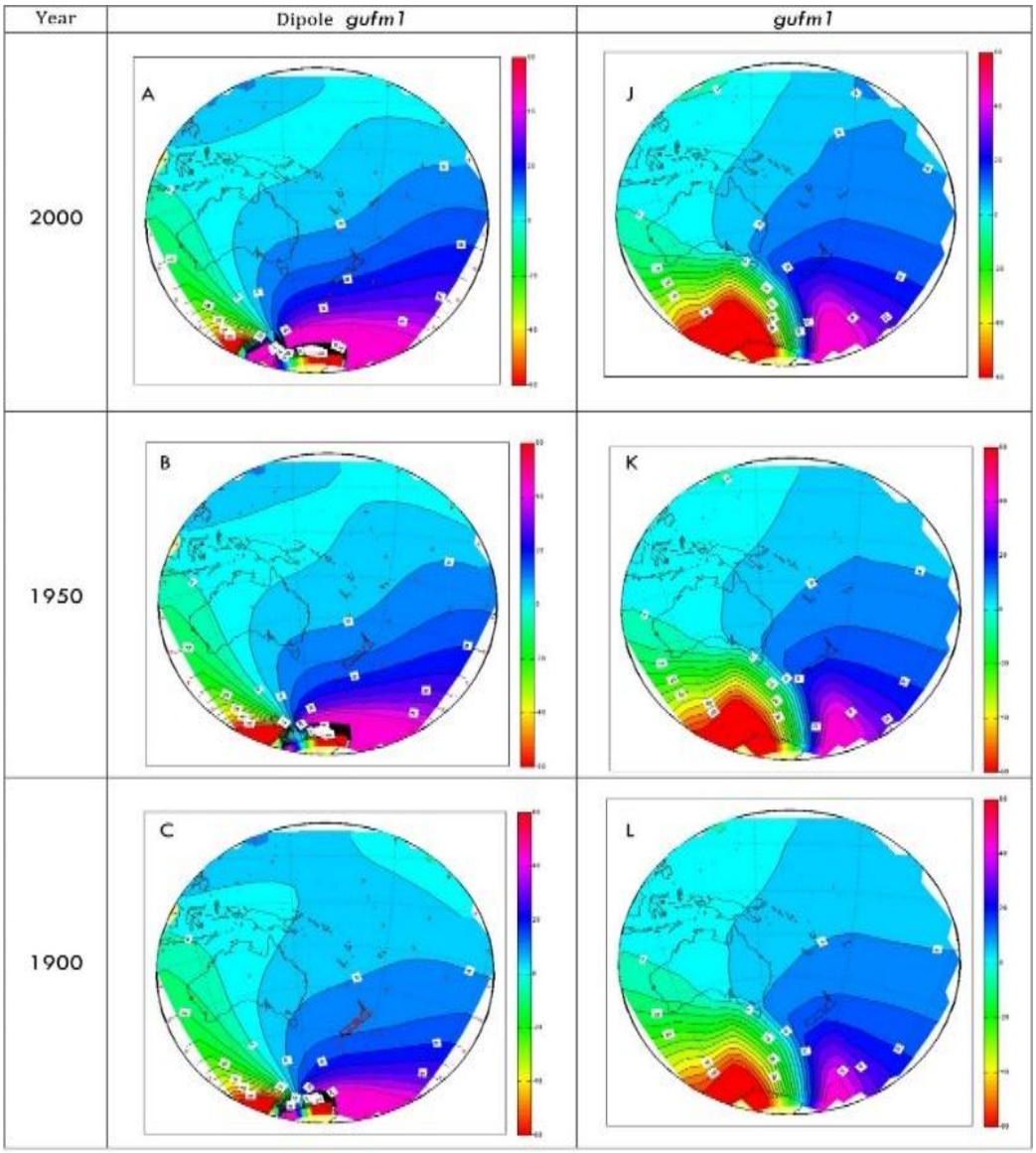

Year	Dipole *gufm1*	*gufm1*
1875	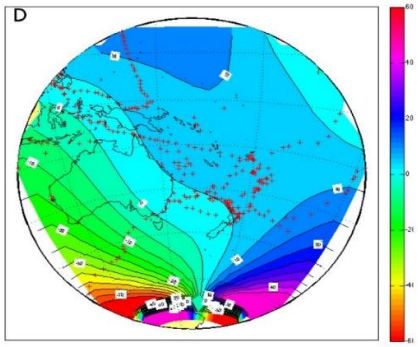	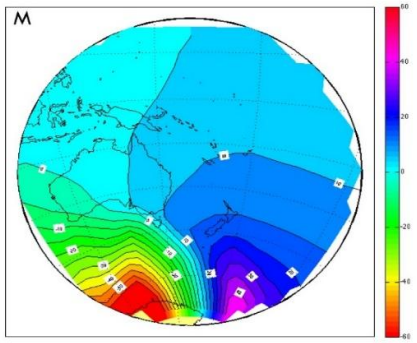
1825	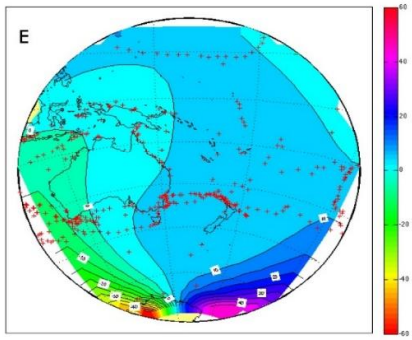	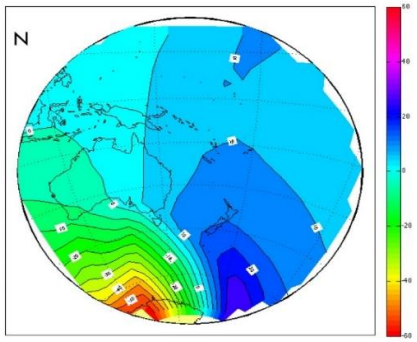
1790	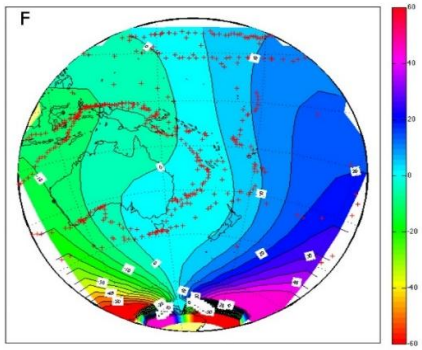	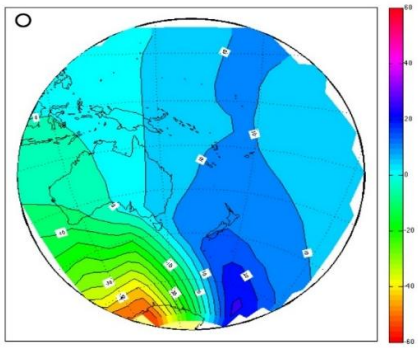
Year	Dipole *gufm1*	*gufm1*
1773	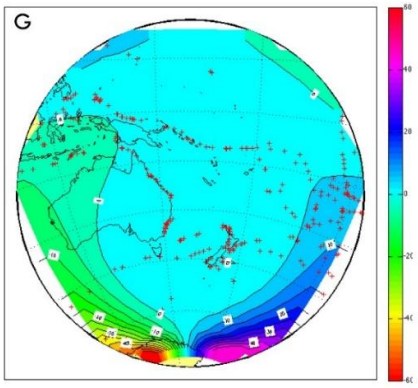	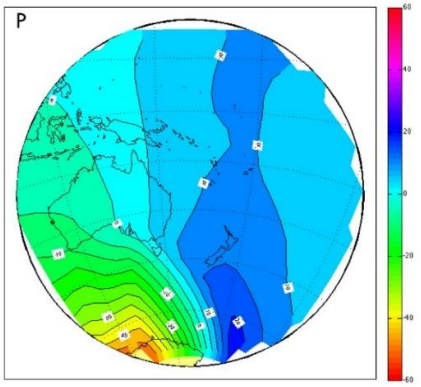

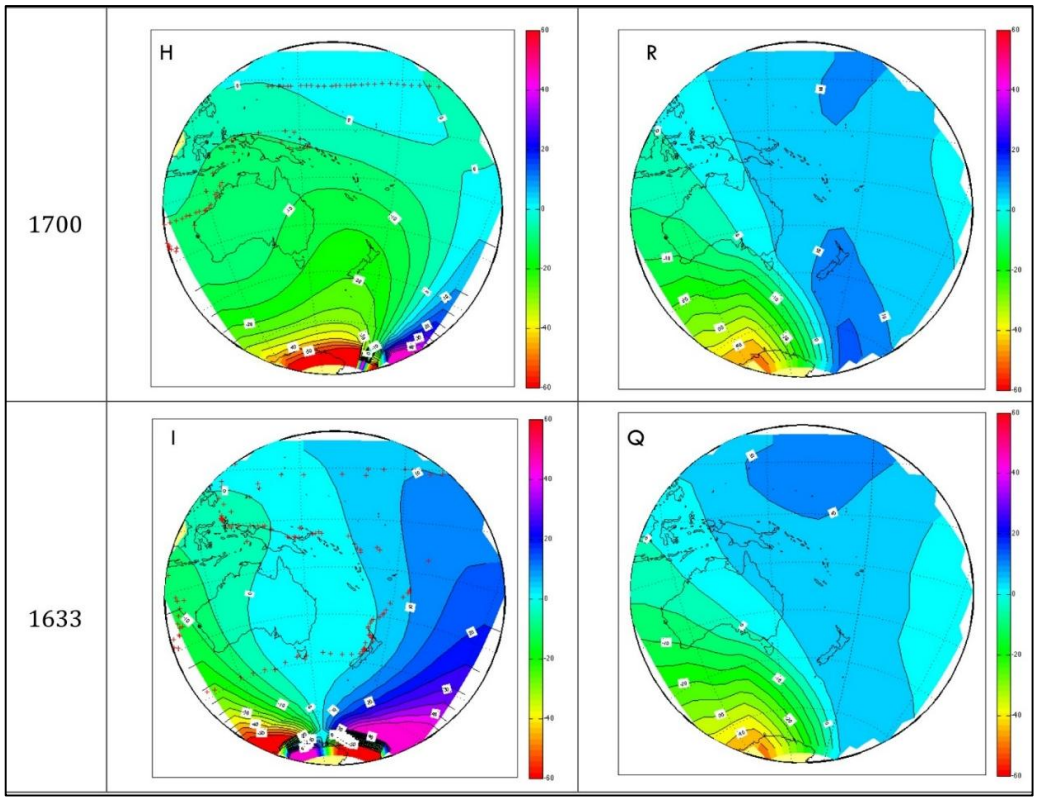

Fig. 4. Declination maps for the southwest Pacific region from 1633 to 2000. Comparing the results of the gufm1 dipole model (A-I) with the gufm1 model (J-R). Contour interval is 5°

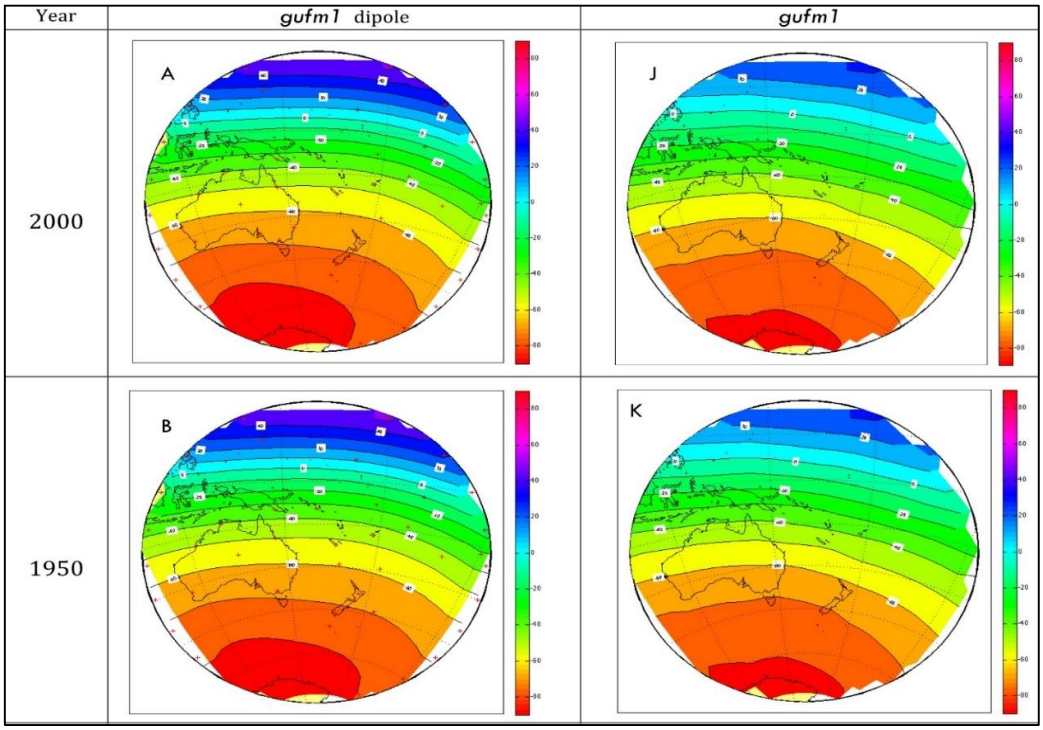

1900	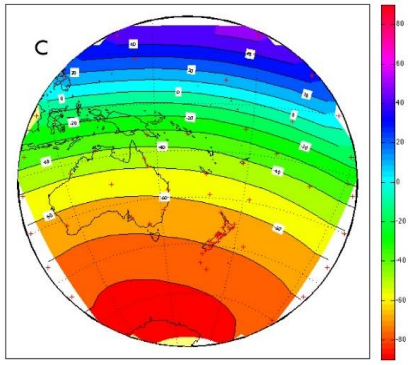	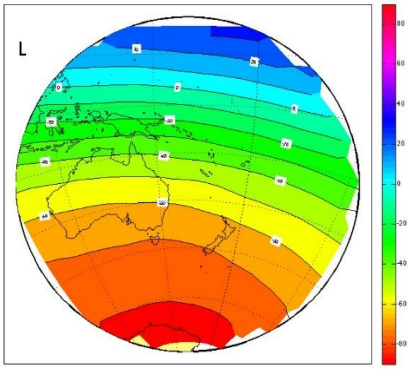
Year	*gufm1* dipole	*gufm1*
1875	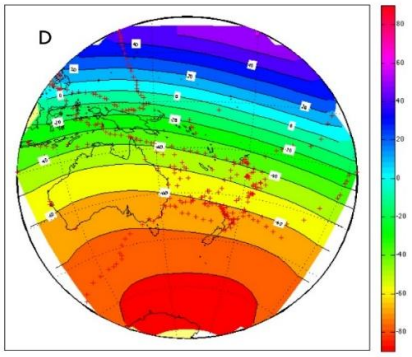	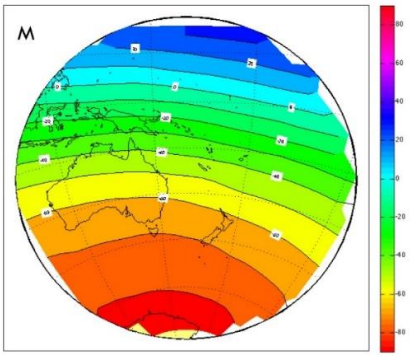
1825	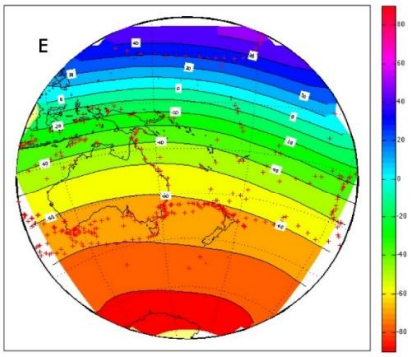	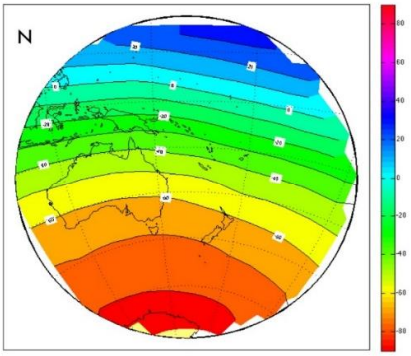
1790	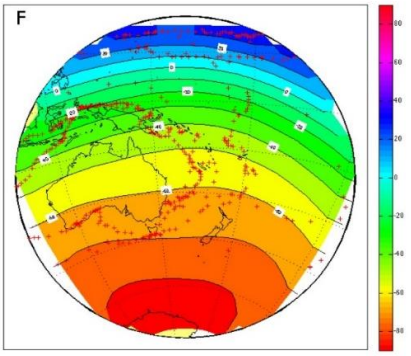	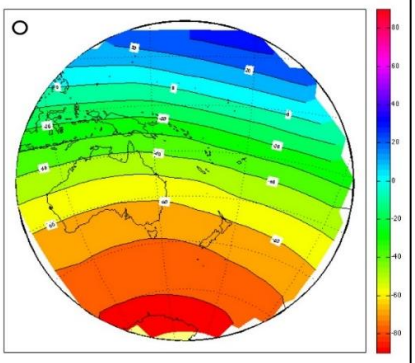

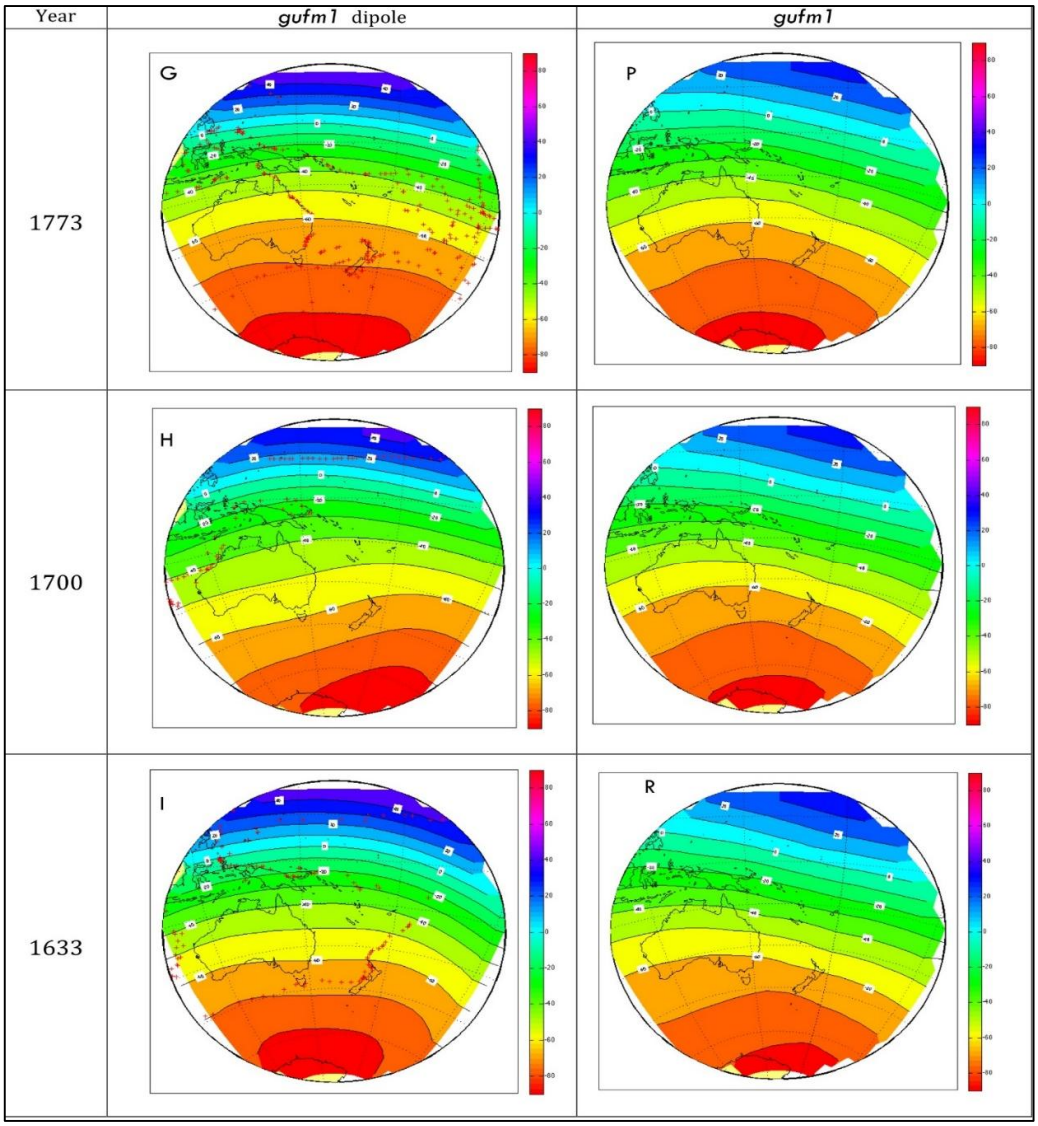

Fig. 5. Inclination maps for the southwest Pacific region from 1633 to 2000. Comparing the results of the gufm1 dipole model (A-I) with the gufm1 model (J-R). Contour interval is 10°

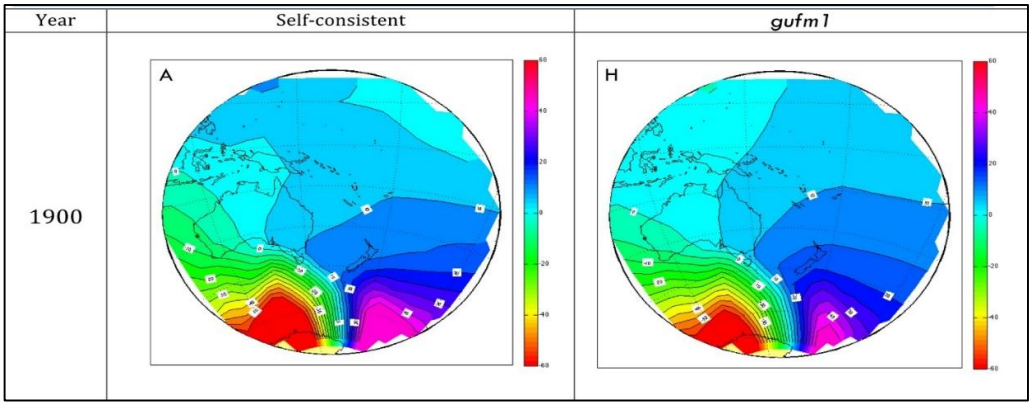

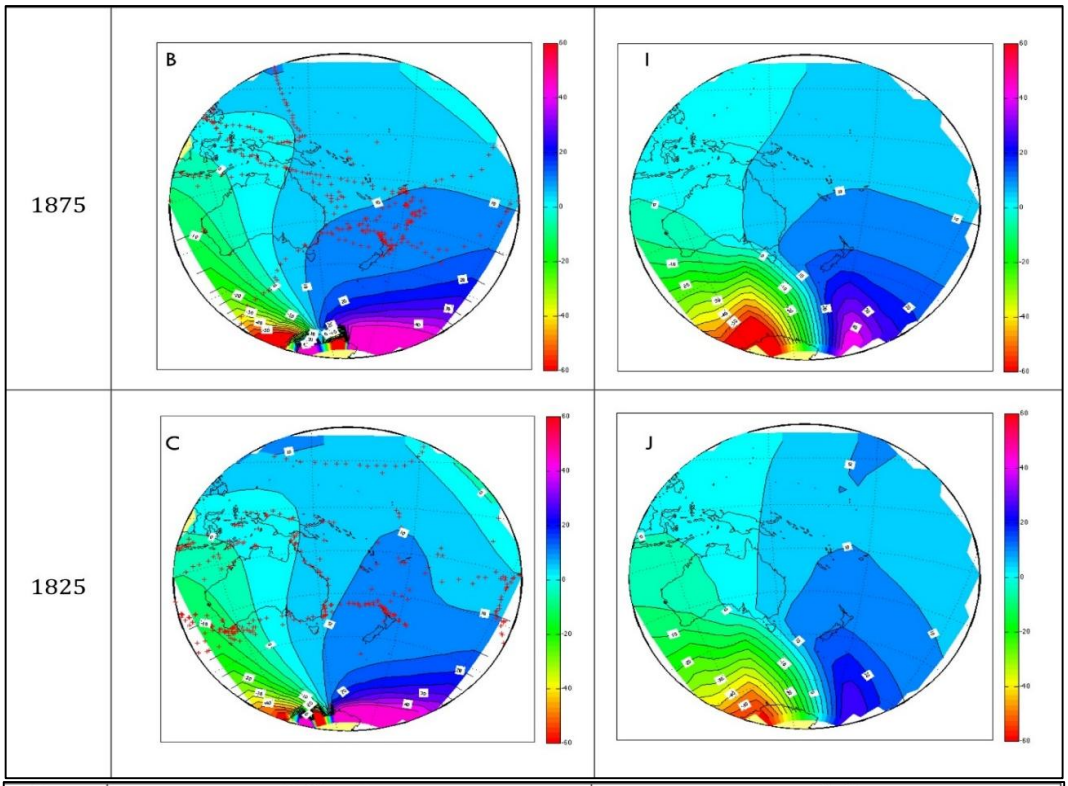

Year	Self-consistent	*gufm1*

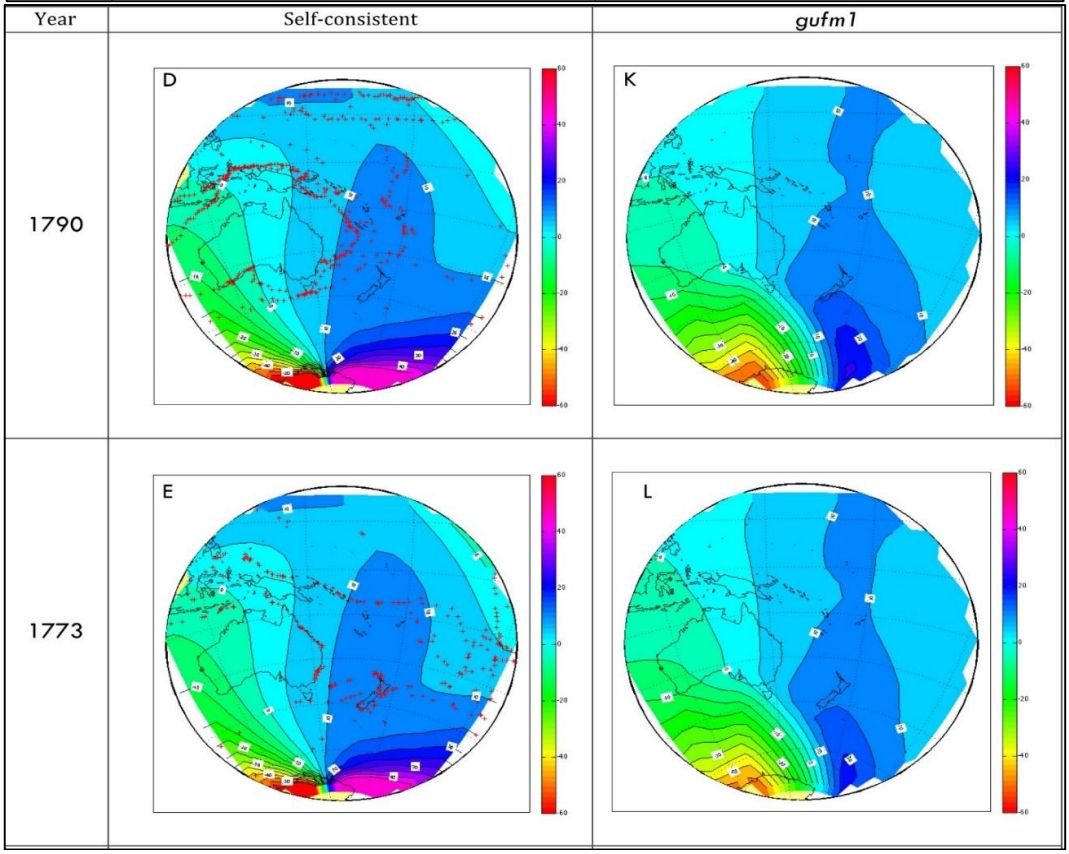

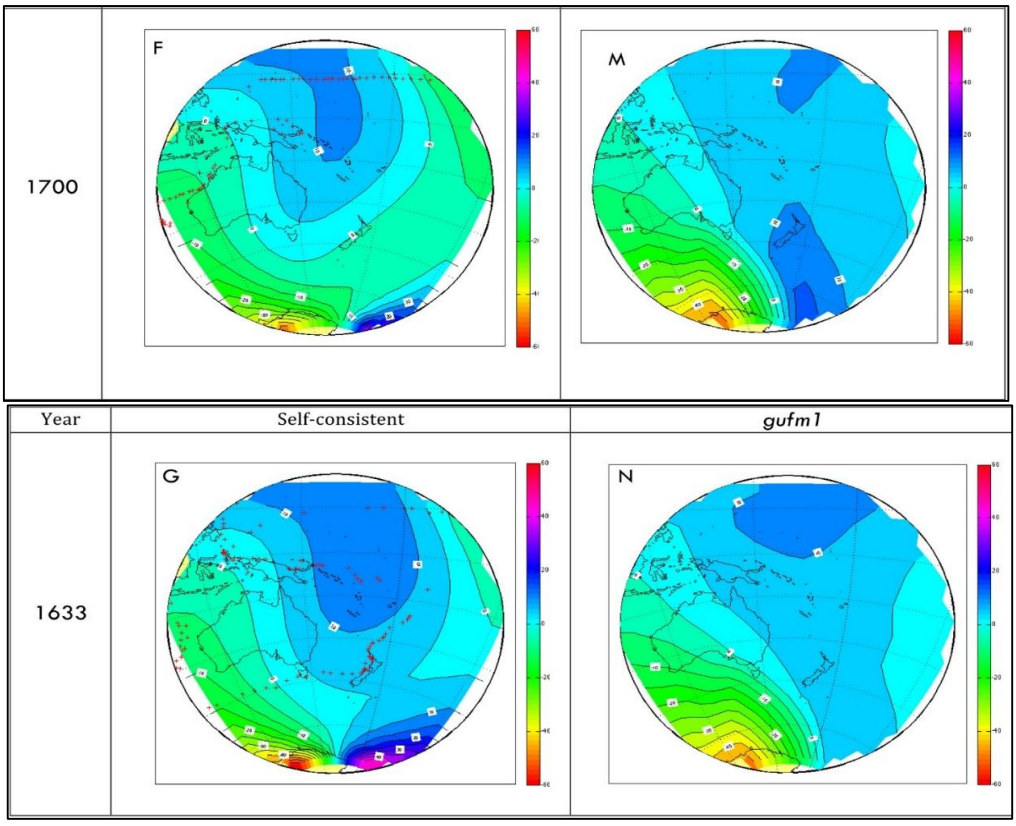

Fig. 6. Declination maps for the southwest Pacific region from 1633 to 1900. Comparing the results of the self-consistent model (A-G) with the gufm1 model (H-N). Contour interval is 5°

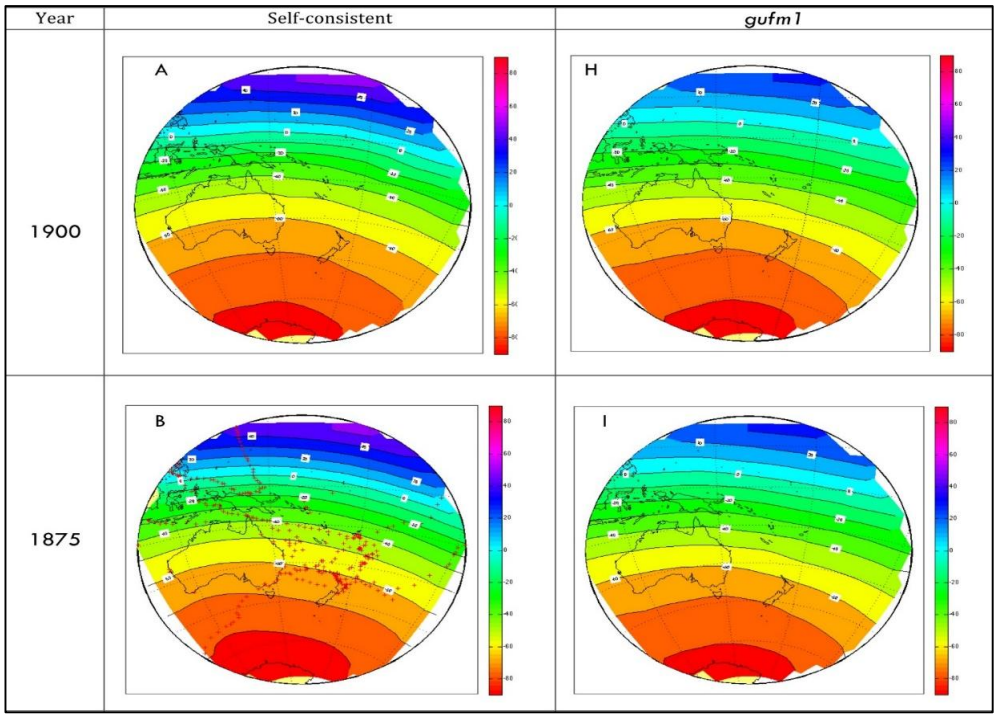

1825	C 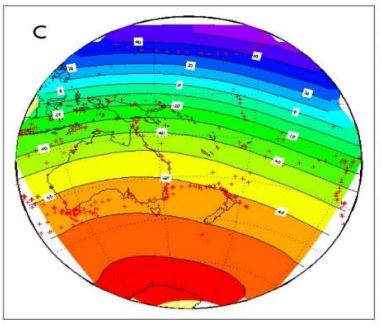	J 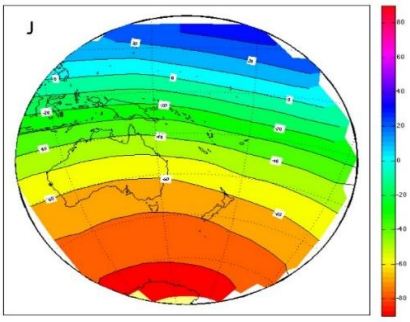
Year	Self-consistent	*gufm1*
1790	D 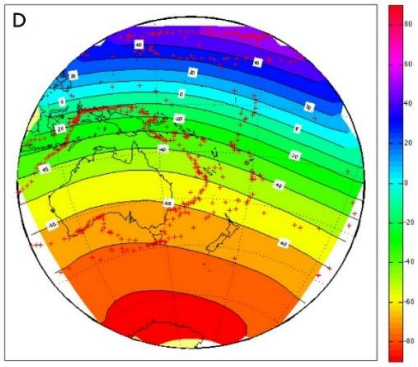	K 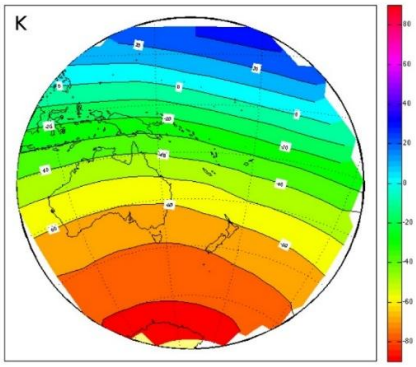
1773	E 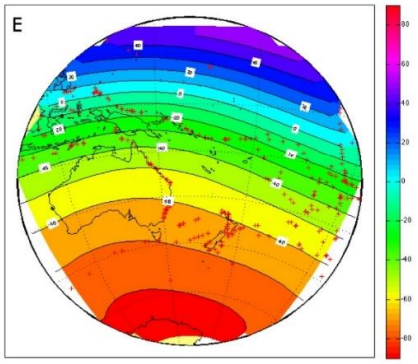	L 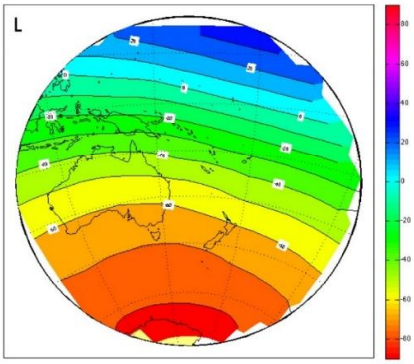
1700	F 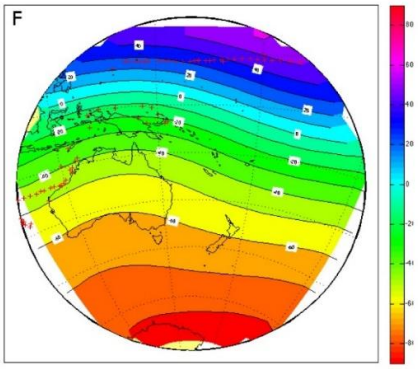	M 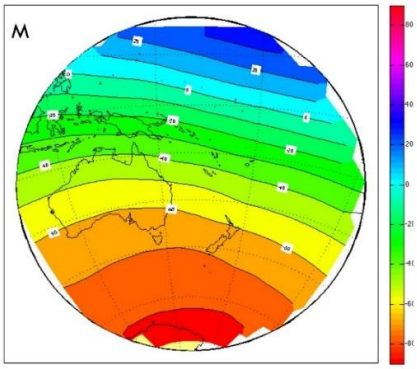

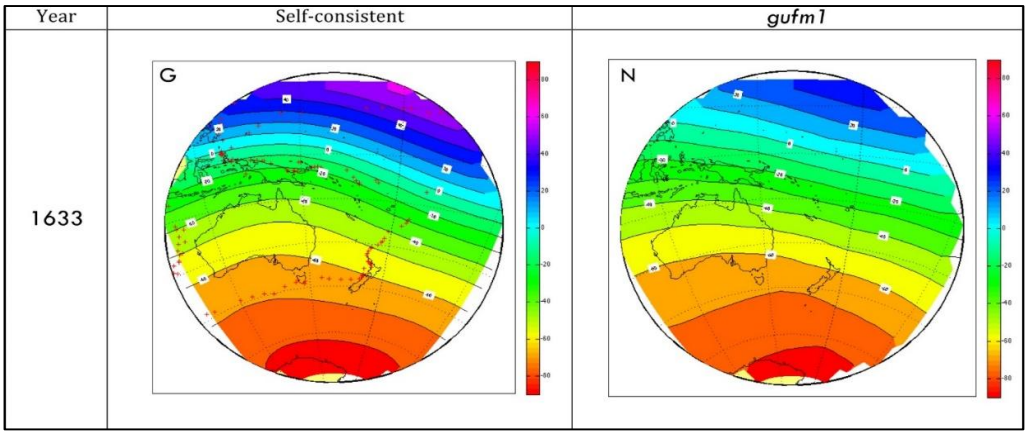

Fig. 7. Inclination maps for the southwest Pacific region from 1633 to 1900. Comparing the results of the self-consistent model (A-G) with the gufm1 model (H-N). Contour interval is 10°

Table 1. The root mean square difference between estimated values (Xe, Ye, Ze) and modeled values at each latitude and longitude of data point for each period of time from 1633 to 1875

Year	*gufm1* dipole model	Self-consistent model
1633	5700 nT	2759 nT
1700	5473 nT	2295 nT
1733	12155 nT	1562 nT
1790	10838 nT	1406 nT
1825	8515 nT	6560 nT
1875	13309 nT	3279 nT

It is clearly apparent from the results in the Table 1 that the calculated root mean square value for the self- consistent model gives significantly smaller values than the gufm1 dipole model. A comparison of root mean square misfits between magnetic field values in the X, Y and Z direction for both models, Table 2, shows that the B_X and B_z magnetic field values for the gufm1 dipole model are the most significant contributions to the magnetic field misfits especially in the historical period from 1633 to 1790. This is clearly visible in the *gufm1* dipole declination contours plots, Fig. 4, as these plots are poor for these epochs and differ from those for the *gufm1* model. As the total magnetic field strength is of the order of 50000 nT, the gufm1 dipole average root mean square difference is up to nearly 40% of the total field, whilst the self-consistent root mean square difference is about 6% only. Therefore, the self-consistent model appears to provide a more reliable model field for our region of interest than dipole *gufm1*.There are a number of important reasons of why the gufm1 dipole model does not give as good a fit to the data values as the self-consistent model. As explained previously, for the *gufm1* dipole model for each epoch the first three coefficients, g_1^0, g_1^1 and h_1^1 of the *gufm1* model were used to compute the missing declination and/or inclination and/or intensity values. The estimated values therefore are based only on the dipolar part of the *gufm1* model and do not consider the non - dipole part of the geomagnetic field in the southwest Pacific region. The self-consistent model was built from a distribution of data within the cap with the aid of a linear extrapolation of SCH Gauss coefficients up to degree 2 that include both the dipolar and non-dipolar parts of the field. The extrapolation also includes reliable IGRF observed data for 2000, 1950 and 1900. Another reason of why one should not put much weight on the *gufm1* dipole model is the uneven distribution of the data sites through the spherical cap in some epochs. An example is the contours of declination for 1700, Fig. 4, where that data aligns linearly across the top of the cap. In contrast with this the use, through extrapolation, of the previous values of SCH coefficients to help fill in data gaps in the self-consistent model means that the effect of poor data distribution on the results is reduced. The only exception to this is the declination plot for 1700, Fig. 6, although this still has some of the features seen for the other epochs.

Table 2. The X, Y and Z root mean squares of gufm1 dipole and self-consistent model from 1633 to 1875

year	ε_x nT		ε_y nT		ε_z nT	
	gufm1 dipole	Self-consistent	*gufm1* dipole	Self-consistent	*gufm1* dipole	Self-consistent
1633	2851	474	3190	2634	3957	668
1700	2437	964	3430	1855	3500	947
1733	9933	566	3820	1398	5873	405
1790	9051	613	3209	1277	5025	311
1825	3142	2089	2251	982	7587	6140
1875	8545	1988	2096	1227	9986	2301

4. CONCLUSION

In this study, two regional model of the geomagnetic field for the southwest Pacific region have been developed covering the time span from1600 to 2000. Both models have been calculated by using the SCHA regional technique. These models have been calculated using observational and estimated declination and inclination for different epochs. Also, research was determining the best geomagnetic field model in the southwest Pacific region for the last 400 years. Observations of all three magnetic field components are required in order to produce a model for the field. Where data gaps occur unrecorded values of inclination and declination at a site have been calculated using the geocentric dipole components from the *gufm1* global model. Analysis of these data gives the *gufm1* dipole model. Maps for the geomagnetic field for this model suggest that this model does not give a good representation of the geomagnetic field in southwest Pacific region. A self- consistent model has been obtained from linear extrapolation of SCHA Gauss coefficients up to *l=2* derived initially from 2000, 1950 and 1900 IGRF observed data. The extrapolation has then been applied further back in time to seven different epochs. The magnetic field plots show that this model gives a much closer fit to the gufm1 model which is the best historical global model since 1600. The results suggest that the self-consistent model provides a more reliable model field for the southwest Pacific region than the *gufm1* dipole model. The root mean squared misfit of the self-consistent model to the field values averages 2900 nT, compared to 23000 nT for the *gufm1* dipole model.

COMPETING INTERESTS

Authors have declared that no competing interests exist.

REFERENCES

1. Matts DC. The theory of magnetism: An introduction to the study of cooperative phenomena: Harper & Row; 1965.
2. Merrill RT, McElhinny MW, McFadden PL. The magnetic field of the earth: Paleomagnetism, the core and the deep mantle: Academic Press; 1998.
3. Parkinson WD. Introduction to geomagnetism. Scottish Academic Press; 1983.
4. Bloxham J, Gubbins D. The secular variation of Earth's magnetic field. Nature. 1985;317:777-781.
5. Haines GV. Spherical cap harmonic analysis. Journal of Geophysical Research. 1985;90:2583-2591
6. Alldredge LR. Varying geomagnetic anomalies and secular variation. Journal of Geophysical Research: Solid Earth. 1983; 88(B11):9443-9451. Available:https://10.1029/JB088iB11p09443
7. Jackson A, Jonkers AR, Walker MR. Four centuries of geomagnetic secular variation from historical records. Philosophical Transactions: Mathematical, Physical and Engineering Sciences. 2000;358(1768): 957-990. Avialable:https://10.1098/rsta.2000.0569
8. Blakely RJ. Potential theory in gravity and magnetic applications. Cambridge: Cambridge University Press; 1996.
9. Torta JM, Gaya-Piqu ÉL, De Santis A. Spherical cap harmonic analysis of the geomagnetic field with application for aeronautical mapping. In J. Rasson & T. Delipetrov (Eds.), Geomagnetics for Aeronautical Safety: Springer Netherlands. 2006;291-307.
10. Korte M, Haak V. Modelling European magnetic repeat station and survey data by SCHA in search of time-varying anomalies.

Physics of the Earth and Planetary Interiors. 2000;122(3):205-220.
11. Hwang C, Chen SK. Fully normalized spherical cap harmonics: application to the analysis of sea-level data from TOPEX/ POSEIDON and ERS-1. Geophysical Journal International. 1997;129(2):450-460.
12. Ingham. The geomagnetic field in the south pacific during the 19th century New Zealand: Victoria University of wellington; 2009.
13. Jonkers AR, Walker MR. Four centuries of geomagnetic secular variation from historical records. Philosophical Transactions: Mathematical, Physical and Engineering Sciences. 2000;358(1768): 957-990.
Available:https://10.1098/rsta.2000.0569
14. Gubbins D. Can the Earth's magnetic field be sustained by core oscillations? Geophysical Research Letters. 1975;2(9): 409-412.
Available:https://10.1029/GL002i009p00409
15. Turner G. North Pole, South Pole: The epic quest to understand the great mystery of the Earth's magnetism / Gillian Turner. Wellington, N.Z: Awa Press; 2010.
16. Lilley FEM, Day AA. D'Entrecasteaux, 1792: Celebrating a bicentennial in geomagnetism. Eos, Transactions American Geophysical Union. 1993;74(9): 97-103.
Available:https://10.1029/93EO00168
17. Sabine E. Report on the variations of the magnetic intensity observed at different points of the earth's surface: Richard and John E. Taylor; 1838.
18. De Labillardière JJH. Voyage in search of La Pérouse: John Stockdale; 1800.
19. Bemmelen V. Abel Janszoon Tasman's Journal of his discovery of Van Diemen's Land and New Zealand in 1642: With documents relating to his exploration of Australia in 1644: being photo-lithographic facsimiles of the original manuscript: With an English translation to which are added Life and labours of Abel. By J.E. Heeres and Observations made with the compass by. Amsterdam: Frederik Muller; 1898.
20. Barton C, McElhinny M. A 10 000 yr. geomagnetic secular variation record from three Australian maars. Geophysical Journal International. 1981;67(2):465-485.
21. Turner GM, Lillis DA. A palaeomagnetic secular variation record for New Zealand during the past 2500 years. Physics of the Earth and Planetary Interiors. 1994; 83(3–4):265-282.
Available:http://dx.doi.org/10.1016/0031-9201(94)90093-0

Peer-review history:
The peer review history for this paper can be accessed here:
http://www.sdiarticle4.com/review-history/51494